

# **Where does the time go: mixing and the depth-dependent distribution of fossil ages**

Rebecca C. Terry & Mark Novak

## **Supplemental Information**

- I. Comparison with survivorship-only models
- II. Model implementation
- III. Additional distribution moments
- IV. Background on Homestead Cave, Utah
- V. Testing for a taphonomic clock
- VI. AMS  $^{14}\text{C}$  procedure details and data table
- VII. Supplemental figures
- VIII. Supplemental references

## I. Comparison with survivorship-only models

Previous efforts to model specimen age-frequency distributions have implicitly conflated time and specimen age, and have not considered depth, mixing or burial explicitly. That is, these efforts have modeled the density of specimens,  $f(a)$ , as

$$\frac{\partial f(a)}{\partial a} = -h(a)f(a),$$

which we call survivorship-only models. The hazard function  $h(a)$  represents the rate (or probability) with which specimens of a given age  $a$  disintegrate, and must either be positive or zero. Typically the hazard rate has been assumed to be independent of specimen age (i.e.  $h(a) = \lambda$ ). More recent models have considered age-dependent Weibull or two-phase hazard functions (Tomašových et al., 2014), though other functions are also possible (e.g., Gompertz-Makeham).

Survivorship-only models can be solved explicitly as

$$f(a) = f_0 e^{-\int_0^a h(\alpha) d\alpha},$$

where  $f(a)$  is the density of specimens of age  $a$  and  $f_0 = f(0)$  is the initial density of zero-aged specimens. This corresponds to exponential decay when the hazard rate is age-independent. The probability that a specimen survives to age  $a$  is given by the survivorship function,

$$S(a) = e^{-\int_0^a h(\alpha) d\alpha},$$

which will always be a non-increasing function of age  $a$  because  $h(a)$  is nowhere negative. The expected age-frequency distribution of specimens is then

$$g(a) = \frac{S(a)}{\int_0^\infty S(a) da}.$$

The denominator corresponds to the mean expected age, which is a constant that makes  $g(a)$  a probability density function.

Since  $g(a)$  is proportional to  $S(a)$  it is also a non-increasing function of age. Consequently, specimen age-frequency distributions with central peaks cannot arise from survivorship-only models. Previous efforts to model age-frequency distributions have therefore had to appeal to unmodeled pulses or decreases in specimen influx rates to explain the relative scarcity of younger specimens (Kowalewski and Rimstidt, 2003; Olszewski, 2012).

## II. Model implementation

We implemented an agent-based formulation of our model in order to investigate its implications for the dynamics of a community's biodiversity as perceived through a fossil record. Zero-aged specimens entered at the surface at rate  $I$ . Rates of burial and mixing were specified using a Normal distribution with mean  $\mu$  (corresponding to a constant burial rate,  $b$ ) and standard deviation  $\sigma$  (corresponding to a constant mixing rate,  $m$ ) -- reflecting the Brownian motion of diffusive mixing -- on which reflecting surface and bedrock boundaries were imposed. Survivorship was specified with a constant hazard rate  $h$  (corresponding to exponential decay). To specify the simplest hypothesis of constant community structure, the identity of specimens deposited on the surface entailed a sequential uniform distribution such that only a single species was present in the "live" community at each time-step. Community richness and evenness of the true "live" community were thus constant in time. The simulation proceeded for a total of  $T$  time

units with time-step intervals set to size  $\Delta t$ . Parameters  $I = 20000$ ,  $\mu = 4.4$ ,  $\sigma = 10$ ,  $d_0 = 0$ ,  $h = 0.02$ ,  $\Delta t = 200$  and  $T = 12800$  were chosen arbitrarily or to reflect the approximate total depth and time of the Homestead Cave record. The final stratigraphic column was sectioned into 20 uniformly spaced layers corresponding roughly to the number of layers evidenced at Homestead Cave. For each layer, 100 specimens were randomly sampled 1000 times to calculate mean and 95% confidence intervals for the apparent richness and evenness of the community. Each stratum's apparent richness and evenness was scaled to the apparent richness and evenness of the surface stratum to standardize comparisons and quantify the magnifying effect of time-averaging on inferred community dynamics.

### III. Distribution moments

We constructed empirical age-frequency distributions for each of the four target strata and obtained mean and 95% credible intervals for distribution moments by sampling from each specimen's posterior probability age distribution. Skewness ( $G_1$ ) and excess kurtosis ( $G_2$ ) were respectively calculated by their population estimators as

$$G_1 = \frac{\sqrt{n(n-1)}}{n-2} \frac{\frac{1}{n} \sum_{i=1}^n (x_i - \bar{x})^3}{\left(\frac{1}{n} \sum_{i=1}^n (x_i - \bar{x})^2\right)^{3/2}}$$

and

$$G_2 = \frac{n-1}{(n-2)(n-3)} \left( (n+1) \left( \frac{\frac{1}{n} \sum_{i=1}^n (x_i - \bar{x})^4}{\left(\frac{1}{n} \sum_{i=1}^n (x_i - \bar{x})^2\right)^2} - 3 \right) + 6 \right)$$

Skewness and kurtosis are not independent descriptions of distribution shape (Fig. DR2). A leptokurtotic distribution having positive excess kurtosis exhibits a more acute peak and heavier tails than a normal distribution.

Histograms and density plots are sensitive to binning and bandwidth choices, particularly at low sample sizes. Further, each estimate of specimen age is associated with an uncertainty expressed by its posterior probability distribution. We therefore used empirical cumulative distributions as a more robust means of visualizing distribution shape. The sensitivity of the relationship between total age range and temporal acuity to specimen outliers was also determined by calculating the age range of all possible subsets of specimens (Fig. DR5).

Down-core changes in the first two moments of age-frequency distribution shape provided less informative tests our model. Mean age, for example, will always increase with depth given non-negative burial and specimen input rates (Fig. DR3A-B). Observed changes in distribution variance, standardized by mean stratum thickness, were generally consistent with model predictions but contained a clear outlier (Fig. DR3C-D). The outlier, Stratum VII, exhibited less variance per cm than predicted by our model. We suspect that this is due to the stratum's distinct sedimentology. While the other strata consist of homogenous layers of silty loam rich in organic remains, stratum VII consists of organic debris interbedded with lenses of eolian or colluvial silt (Madsen, 2000). These lenses likely reflect pulses of wind or water-driven sediment that accumulated rapidly relative to background rates of sediment and organic accumulation. This would translate into an apparent signal of less time captured per unit of stratum thickness, depressing the stratum's age variance.

#### **IV. Background on Homestead Cave, Utah**

Homestead Cave (1406 m elev.) is located just west of the Great Salt Lake in north-central Utah on the northwestern-most spur of the Lakeside Mountains (Fig. DR4). The taphonomy of Homestead Cave reflects a common pathway by which small mammal skeletal remains enter the Quaternary fossil record: owl predation (Grayson, 2000; Terry, 2007). Surface deposits of these small mammal assemblages have been shown to record ecological data, such as species richness, evenness and relative species abundances, with high fidelity (Terry, 2010a; Terry, 2010b), as have the surface deposits of many other taphonomic and depositional settings (Kidwell, 2002; Western and Behrensmeyer, 2009; Miller, 2011; Tomašových and Kidwell, 2011).

A 1 x 1 m column was excavated to bedrock by D.B. Madsen and D.K. Grayson in 1993, with 18 separate strata being removed while respecting natural stratigraphic boundaries defined by changes in sedimentology (Madsen, 2000). Twenty-one radiocarbon dates (both conventional and AMS) associated with organic material from these strata indicate that the Homestead Cave record spans  $13,188 \pm 102$  calendar years (from the late Pleistocene to the present)(Madsen, 2000). However, these dates were not conducive to evaluation of our model because they are primarily sourced from artiodactyl fecal pellets and hackberry endocarps that likely have higher and more varied rates of decomposition and decay than do bones. We instead used femora belonging to *Dipodomys microps* and *D. ordii*, two co-occurring kangaroo rats of comparable size. Bone breakage patterns have shown the cave's deposits to have been produced by large owls for the duration of its depositional history (Terry, 2007). We collected modern deposits from the surface of the cave floor directly adjacent to the excavation column in 2004 (Terry, 2010; Terry et al., 2011).

#### **V. Testing for a Taphonomic Clock**

Determining the ages of many specimens across a stratigraphic sequence is often both logistically infeasible and cost prohibitive. Patterns of specimen damage accrual have been suggested as low-cost indicators of specimen age that also permit insight into the mechanisms of specimen loss.

We scored each bone by its taphonomic condition prior to AMS  $^{14}\text{C}$  analysis. Taphonomic categories were based on Terry (2004) and described the degree of bone modification as follows: (1) unmodified - intact outer layer of dense compact bone, (2) slightly modified - outer layer of compact bone is still intact but pitted in areas and bone edges slightly rounded, (3) modified - inner cancellous bone is exposed in areas, and (4) heavily modified - inner cancellous bone is exposed and eroded. The measure describes the outward appearance of a bone and was not meant to be a comprehensive assessment of potential physical and chemical sources of bone alteration.

Unfortunately, we observed no relationship between a specimen's taphonomic condition and its age at Homestead Cave, both within and across strata (Fig. DR7). Indeed, weathering rates appear highly variable at the decadal to millennial time-scales of our study. This result contrasts with relationships seen in modern decadal-scale studies of large-bodied vertebrate bones (Behrensmeyer, 1978; Behrensmeyer, 1982; Miller, 2011), but mirrors annual to

millennial-scale studies in marine systems that have shown the “taphonomic clock” approach to be unreliable (Flessa et al., 1993; Carroll et al., 2003; Kidwell et al., 2005; Kosnik et al., 2007). The development of lower-cost dating techniques for Quaternary terrestrial fossils should thus be considered a priority.

## VI. AMS <sup>14</sup>C procedure details and data table

AMS <sup>14</sup>C dating was conducted on purified bone collagen. Within each stratum, selected femora were restricted to either the left or right side to avoid the possibility of selecting two bones from the same individual, but were otherwise selected at random with respect to taphonomic condition. Analyses were performed at the University of Arizona Accelerator Facility (AA samples) and the Center for Accelerator Mass Spectrometry at Lawrence Livermore National Laboratory (CAMS samples) (see Table DR1), with standard acid pretreatment procedures following Longin (1971). Collagen preservation was typically high (7%–20%), with only four samples returning anomalously low collagen yields ( $\leq 1\%$ ). These dates were excluded from our analyses.

Table DR1. AMS <sup>14</sup>C dates from bone collagen obtained from Kangaroo Rat femora from Homestead Cave, Utah. Dates were calibrated using OxCal 4.1 and the IntCal 09 and Bomb04NH calibration curves. Modal calibrated age represents the highest probability peak obtained from the Bayesian posterior probability distribution associated with date calibration.

Sample	Stratum	$\delta^{13}\text{C}$	Fraction Modern	$\pm$	Radiocarbon Age		Calibrated Age (cal yrs before AD2000)			Bone Modification Score
					Age	1 $\sigma$	Modal Age	2 $\sigma$ Range		
CAMS137143	Surface	-14	1.3024	0.0051	>Mod.		20.9	20	41	2
CAMS137144	Surface	-14	1.3254	0.0064	>Mod.		21.9	21	24	4
CAMS137185	Surface	-14	1.2932	0.0050	>Mod.		20.7	20	41	1
CAMS137145	Surface	-14	1.2789	0.0050	>Mod.		19.7	19	41	3
CAMS137146	Surface	-14	1.0791	0.0042	>Mod.		42.9	0	44	2
CAMS137147	Surface	-14	0.9906	0.0039	75	35	104.5	72	315	1
CAMS137148	Surface	-14	1.3257	0.0051	>Mod.		21.9	21	24	1
CAMS136716	Surface	-14	1.3188	0.0087	>Mod.		21.1	21	24	1
CAMS136717	Surface	-14	1.2994	0.0086	>Mod.		20.3	20	41	1
CAMS136718	Surface	-14	1.2780	0.0085	>Mod.		19.7	19	41	2
CAMS136719	Surface	-14	1.3152	0.0093	>Mod.		21.1	21	38	1
CAMS136720	Surface	-14	1.2916	0.0086	>Mod.		20.7	20	41	1
CAMS136721	Surface	-14	1.3008	0.0086	>Mod.		20.9	20	41	4
CAMS136722	Surface	-14	1.2966	0.0086	>Mod.		20.7	20	41	2
CAMS136723	Surface	-14	1.3215	0.0088	>Mod.		21.1	21	24	1
CAMS136724	Surface	-14	1.1265	0.0042	>Mod.		5.7	0	43	4
CAMS136726	Surface	-14	0.9727	0.0036	220	35	209.5	45	471	2

CAMS139425	Surface	-14	1.2727	0.0045	>Mod.		19.3	19	41	1
CAMS139426	Surface	-14	1.1051	0.0042	>Mod.		2.9	0	43	1
CAMS139427	Surface	-14	1.2772	0.0049	>Mod.		19.7	19	41	1
AA69314	XV	-10.8	0.7351	0.0045	2472	48	2734.5	2413	2766	1
AA69315	XV	-14.1	0.7509	0.0043	2302	78	2389.5	2168	2748	2
*AA69316	XV	-17.3	0.3809	0.0061	7750	130	8594.5	8401	9032	3
AA72773	XV	-14.1	0.7272	0.0042	2559	46	2784.5	2538	2811	2
AA72774	XV	-11.1	0.7725	0.0043	2073	44	2054.5	1977	2200	1
AA72775	XV	-14.4	0.7585	0.0042	2220	44	2214.5	2185	2390	2
AA72776	XV	-11.4	0.7278	0.0042	2553	46	2774.5	2537	2809	2
AA72777	XV	-12.1	0.9089	0.0047	767	41	734.5	709	815	4
AA72778	XV	-13	0.7319	0.0043	2508	46	2754.5	2416	2794	1
AA72779	XV	-12	0.7904	0.0044	1890	45	1874.5	1766	1976	3
AA72780	XV	-11.3	0.6857	0.0042	3031	48	3299.5	3128	3411	2
AA72781	XV	-14.5	0.7014	0.0042	2850	48	3009.5	2898	3193	4
AA72782	XV	-11.5	0.7589	0.0043	2216	45	2214.5	2180	2388	1
AA72783	XV	-11.6	0.7563	0.0043	2244	45	2364.5	2202	2393	4
AA72784	XV	-12.6	0.7585	0.0044	2221	46	2214.5	2182	2390	3
AA72786	XV	-11.2	0.7126	0.0035	2722	39	2839.5	2804	2970	4
AA72787	XV	-11.3	0.5689	0.0039	4531	54	5199.5	5029	5486	1
AA72788	XV	-8.2	0.7279	0.0035	2551	39	2774.5	2540	2805	2
AA72789	XV	-11.2	0.7569	0.0044	2237	46	2359.5	2200	2392	4
AA72785	XV	-12	-	-	2500	46	2624.5	2416	2790	1
CAMS136728	VII	-14	0.4350	0.0019	6685	40	7619.5	7525	7670	3
CAMS136729	VII	-14	0.4578	0.0020	6275	35	7294.5	7080	7325	1
CAMS136730	VII	-14	0.4595	0.0020	6245	40	7219.5	7068	7312	3
CAMS136731	VII	-14	0.4485	0.0019	6440	35	7384.5	7340	7478	3
CAMS136732	VII	-14	0.4488	0.0020	6435	40	7384.5	7329	7476	4
CAMS136733	VII	-14	0.4526	0.0026	6370	50	7324.5	7227	7472	1
CAMS136734	VII	-14	0.4324	0.0020	6735	40	7634.5	7565	7719	1
CAMS136735	VII	-14	0.4181	0.0019	7005	40	7889.5	7789	7987	2
CAMS134580	VII	-14	0.4643	0.0021	6165	40	7174.5	6999	7218	2
CAMS134581	VII	-14	0.4534	0.0020	6355	40	7319.5	7224	7468	2
CAMS134582	VII	-14	0.4357	0.0017	6675	35	7619.5	7531	7657	4
CAMS134583	VII	-14	0.4539	0.0016	6345	30	7314.5	7222	7463	2
CAMS134584	VII	-14	0.4384	0.0022	6625	45	7604.5	7485	7625	3
CAMS134585	VII	-14	0.4272	0.0017	6830	35	7719.5	7641	7776	1
CAMS134586	VII	-14	0.4539	0.0018	6345	35	7314.5	7221	7464	4
CAMS134587	VII	-14	0.4383	0.0018	6625	35	7604.5	7490	7623	2
CAMS134588	VII	-14	0.4478	0.0019	6455	35	7394.5	7343	7482	1

CAMS134589	VII	-14	0.4512	0.0021	6395	40	7364.5	7314	7470	1
CAMS134590	VII	-14	0.4450	0.0017	6505	35	7474.5	7374	7533	2
CAMS134591	VII	-14	0.4646	0.0019	6160	35	7174.5	7009	7213	1
*AA69311	II	-16	0.307	0.057	9490	1480	10764.5	7874	16220	1
*AA69312	II	-18.7	0.31	0.03	9420	780	10724.5	9046	13116	2
*AA69313	II	-20.1	0.408	0.035	7210	690	8059.5	6726	9938	3
CAMS134592	II	-14	0.4145	0.0017	7075	35	7934.5	7889	8018	3
CAMS134593	II	-14	0.2771	0.0013	10310	40	12134.5	12028	12431	1
CAMS134594	II	-14	0.3479	0.0015	8480	35	9539.5	9500	9595	2
CAMS134595	II	-14	0.3074	0.0014	9475	40	10759.5	10633	11117	2
CAMS134596	II	-14	0.2796	0.0013	10235	40	12039.5	11820	12159	4
CAMS134597	II	-14	0.2940	0.0013	9835	40	11284.5	11245	11365	4
CAMS134598	II	-14	0.2742	0.0013	10395	40	12379.5	12135	12471	1
CAMS141271	II	-14	0.3421	0.0015	8615	35	9594.5	9578	9715	3
CAMS141272	II	-14	0.3058	0.0013	9515	40	10809.5	10714	11129	2
CAMS141273	II	-14	0.2809	0.0012	10200	40	11894.5	11805	12115	1
CAMS141274	II	-14	0.3102	0.0016	9405	45	10704.5	10568	10789	4
CAMS141275	II	-14	0.2822	0.0012	10165	40	11874.5	11695	12083	2
CAMS141276	II	-14	0.2811	0.0012	10195	40	11889.5	11801	12115	1
CAMS141277	II	-14	0.2790	0.0012	10255	35	12084.5	11876	12180	2
CAMS141278	II	-14	0.3144	0.0014	9295	40	10554.5	10348	10695	2
CAMS141279	II	-14	0.3115	0.0013	9370	35	10629.5	10558	10689	4
CAMS141280	II	-14	0.3111	0.0013	9380	35	10689.5	10564	10747	3

\* Specimen excluded from analyses due to low collagen yield.

## VII. Supplemental figures

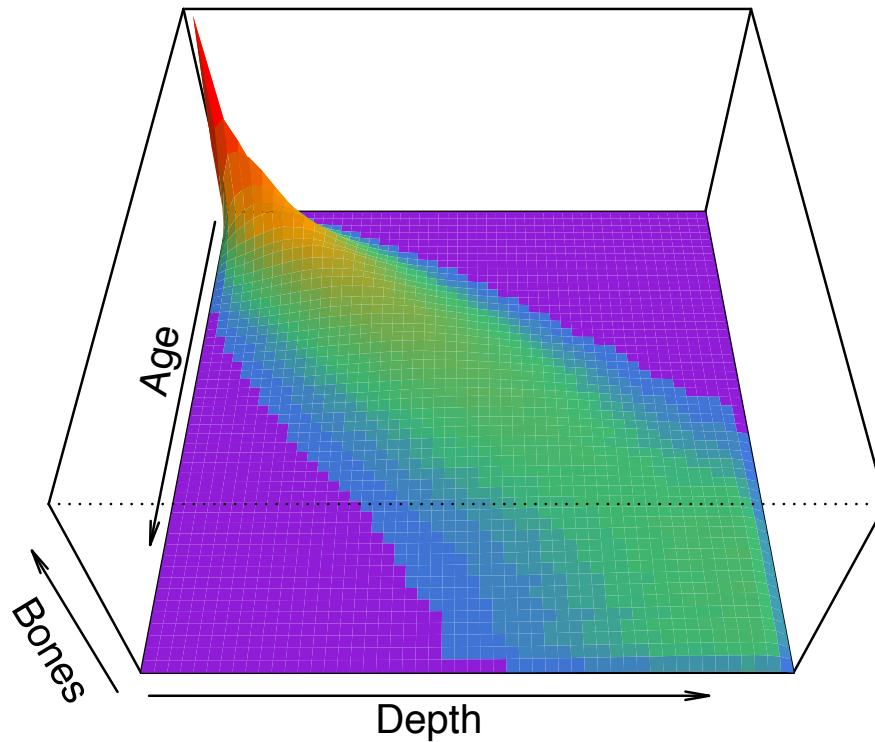


Figure DR1. The predicted frequency of specimens as a function of their depth and age. Parameter values correspond to those in Fig. 1 of the main text. Intuitively, a higher ratio of mixing to burial rates broadens the distribution of depths at which specimens of a given age are found (i.e. flattening the ridge); increasing the ratio of burial to mixing rates affects a steeper ridge. Integrating across all depths (i.e. combining specimens from all depths) to look at only the age-specific density of specimens would show an exponential (constant hazard) survivorship curve.

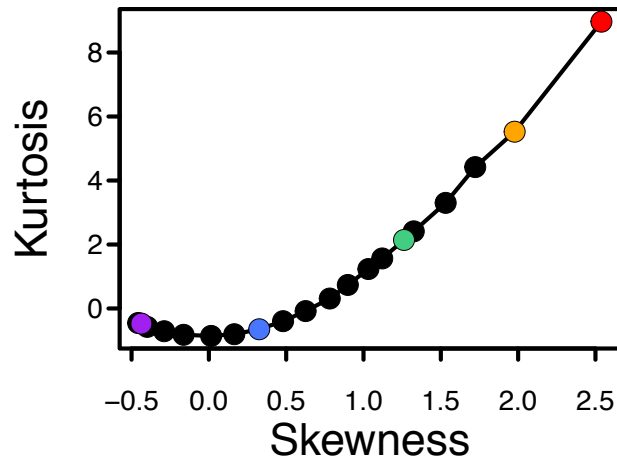


Figure DR2. The predicted relationship between age-frequency distribution skewness and kurtosis across a fossil record's stratigraphic layers showing how these two moments are linked by quadratic dependence. Highly-skewed distributions will also be more leptokurtic. Despite their dependence, skewness and kurtosis quantify different aspects of time-averaging, the former describing where the bulk of time is situated, and the latter describing the distribution's temporal acuity. Color-highlighted layers and parameter values correspond to those in Fig. 1 of the main text. Strata proceed from the surface to increasing depth from right to left.

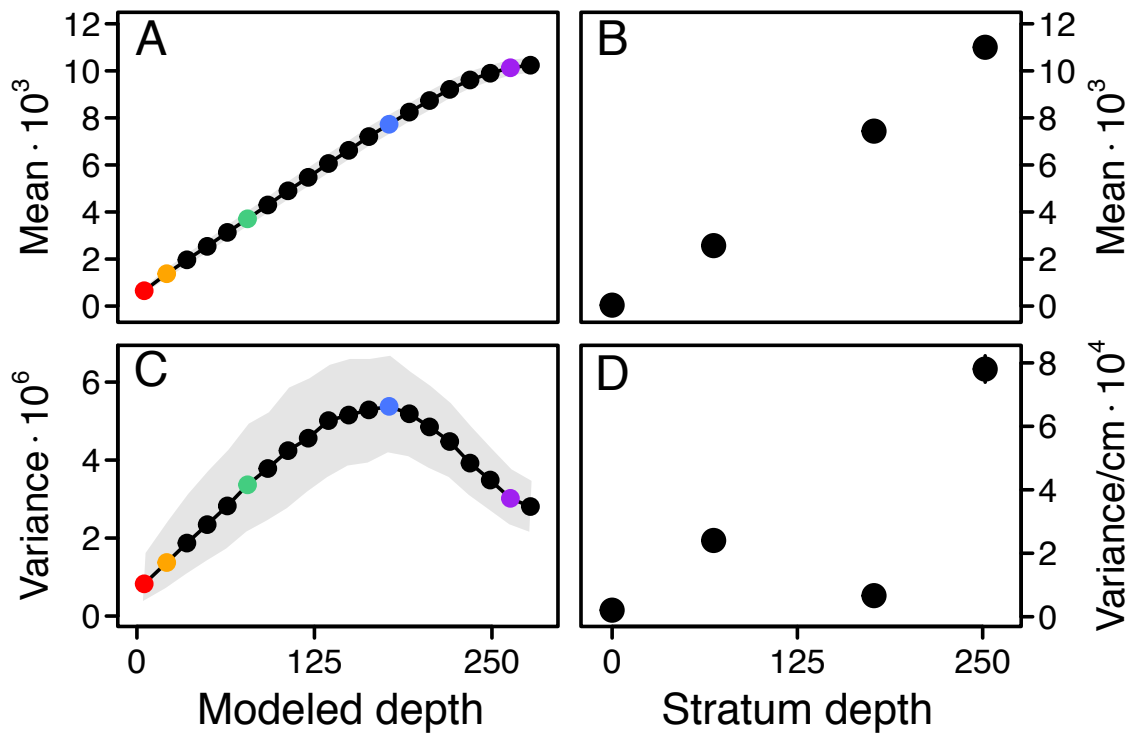


Figure DR3. Predicted (mean and 95% confidence intervals) and observed (posterior mean and 95% credible intervals) down-core changes in distribution mean age (**A**, **B**) and variance (**C**, **D**). Predictions assume that 100 specimens are sampled within each of 20 layers of uniform thickness. Color-highlighted layers and parameter values correspond to those in Fig. 1 of the main text. Empirical variances are standardized by mean stratum thickness (in centimeters).

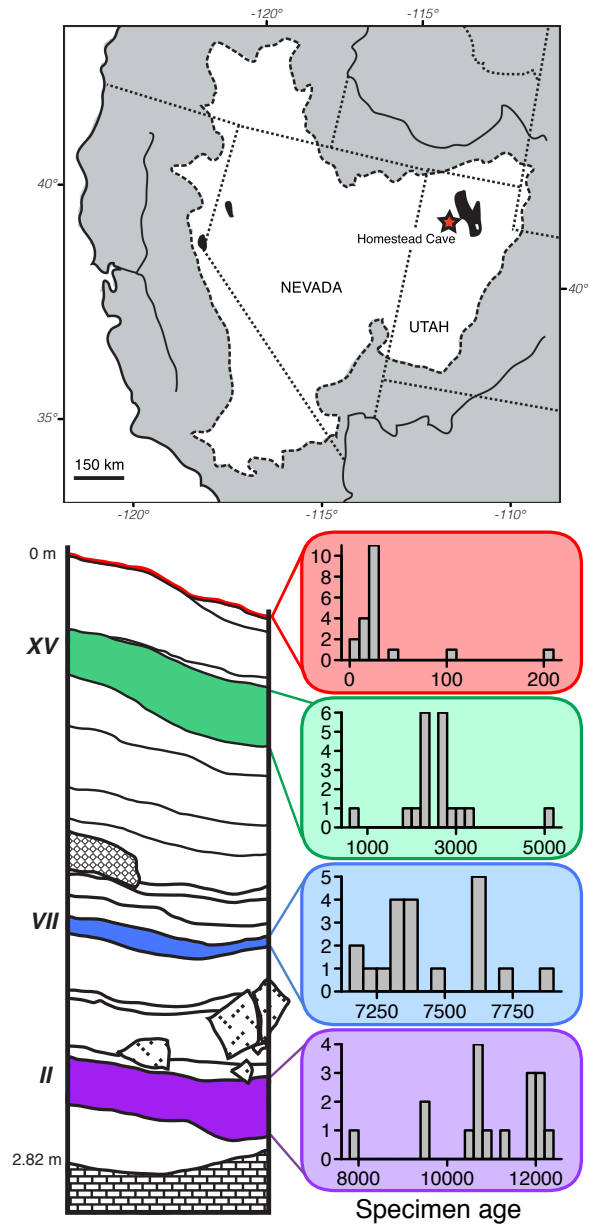


Figure DR4. Observed age-frequency distributions by stratum at Homestead Cave, Utah. Homestead Cave is located just west of the Great Salt Lake. Histograms reflect counts of the specimens' highest posterior probability calibrated ages, adjusted to the year 2000 AD ( $n = 17$  to 20). Map of the Great Basin redrawn from (Grayson, 2000). Stratigraphic column redrawn from (Madsen, 2000).

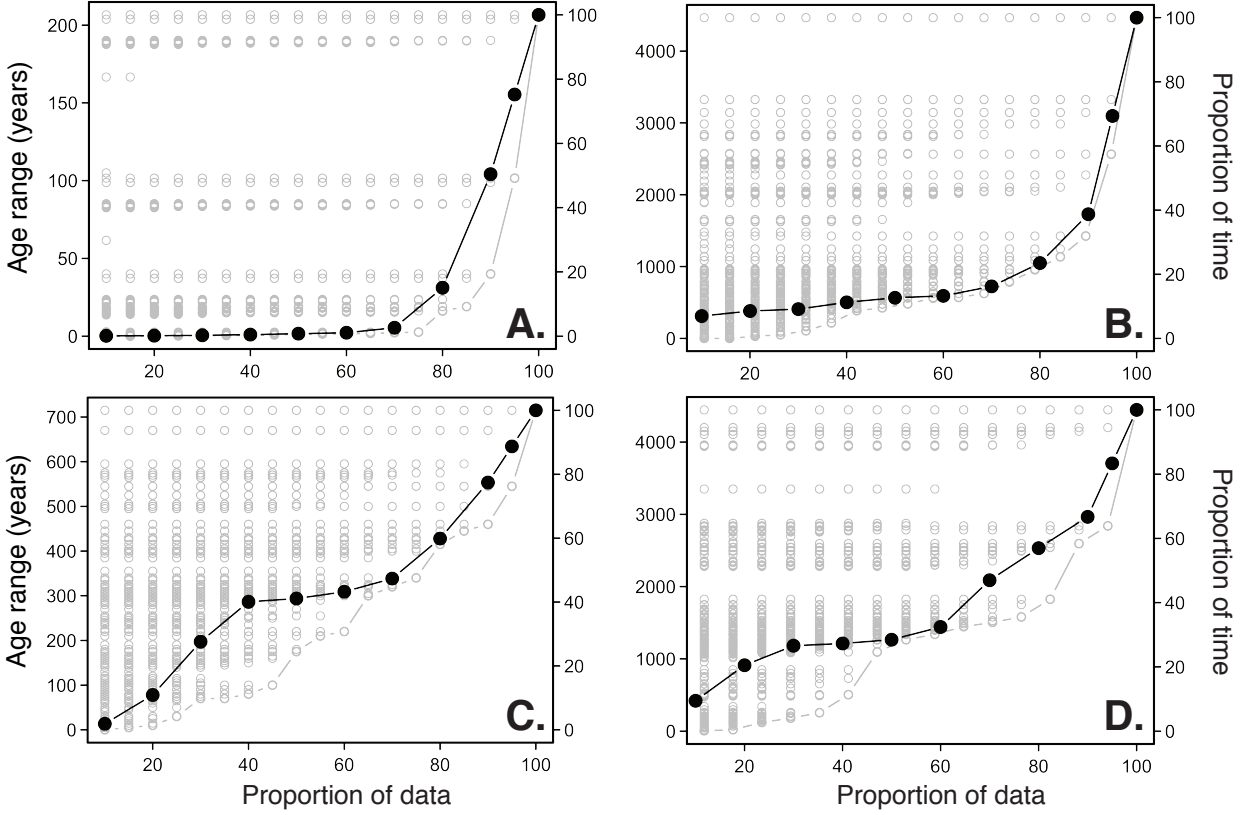


Figure DR5. Sensitivity of each stratum's maximum age range to specimen subsampling. (A) Surface, (B) stratum XV, (C) stratum VII, (D) stratum II. Small circles represent age-ranges obtained from all combinations of varying numbers of excluded specimens (expressed as % of total number of remaining samples per stratum). Filled black circles represent median age-ranges which closely track the boundary of minimum age ranges. Steeper boundaries indicate that more specimens are constrained to a smaller range of ages, resulting in a higher temporal acuity of the stratum. Gaps reflect the degree to which specimen ages are continuous within the age-range window.

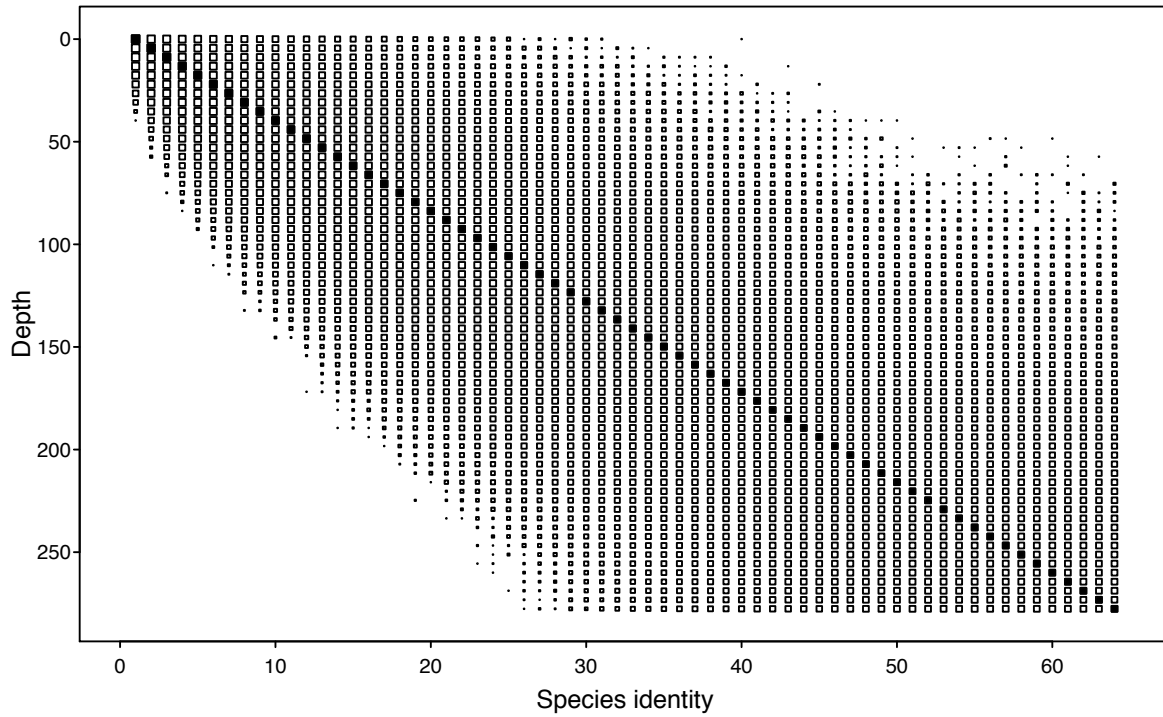


Figure DR6. The process of mixing causes species to occur within sedimentary layers other than the ones in which they were initially deposited. Mixing therefore alters the species diversity of a stratigraphic sequence (and thus perceived community dynamics over time) even when the “live” community producing the record has experienced constant diversity. We simulated constant diversity by having only one species (numbered 1-64) deposited at the surface per time-step (black symbols). Open symbols represent species occurring within other layers due to mixing. Symbol size reflects a species’ frequency at the respective depth. The magnitude of perceived taxonomic turnover through time is dependent on the degree to which non-contemporaneous communities are mixed.

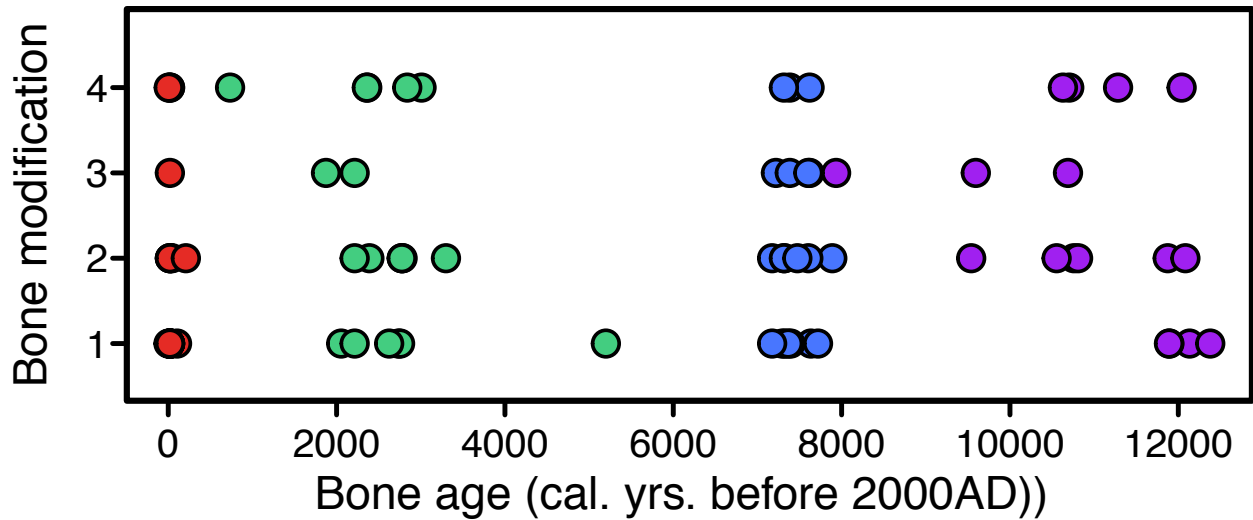


Figure DR7. Relationship between taphonomic condition (bone modification score) and bone age (calibrated years BP), color-coded by stratum as in Fig. DR4. No predictive relationship emerges within or among strata, thus a “taphonomic clock” cannot be used to infer scales of time-averaging in these deposits. Bone modification score was based on Terry (2004) ranging from (1) unmodified to (4) heavily modified.

## VIII. Supplemental references

- Behrensmeyer, A., 1982, Time resolution in fluvial vertebrate assemblages: *Paleobiology*, v. 8, no. 3, p. 211–227.
- Behrensmeyer, A.K., 1978, Taphonomic and ecologic information from bone weathering: *Paleobiology*, p. 150–162.
- Carroll, M., Kowalewski, M., Simoes, M., and Goodfriend, G., 2003, Quantitative estimates of time-averaging in terebratulid brachiopod shell accumulations from a modern tropical shelf: *Paleobiology*, v. 29, no. 3, p. 381–402.
- Flessa, K., Cutler, A.H., and Meldahl, K.H., 1993, Time and taphonomy - quantitative estimates of time-averaging and stratigraphic disorder in a shallow marine habitat: *Paleobiology*, v. 19, no. 2, p. 266–286.
- Grayson, D.K., 2000, Mammalian responses to Middle Holocene climatic change in the Great Basin of the western United States: *Journal of Biogeography*, v. 27, no. 1, p. 181–192.
- Kidwell, S.M., 2002, Time-averaged molluscan death assemblages: Palimpsests of richness, snapshots of abundance: *Geology*, v. 30, no. 9, p. 803–806, doi: 10.1130/0091-7613(2002)030<0803:TAMDAP>2.0.CO;2.
- Kidwell, S.M., Best, M.M.R., and Kaufman, D.S., 2005, Taphonomic trade-offs in tropical marine death assemblages: Differential time averaging, shell loss, and probable bias in siliciclastic vs. carbonate facies: *Geology*, v. 33, no. 9, p. 729–732, doi: 10.1130/G21607.1.
- Kosnik, M.A., Hua, Q., Jacobsen, G.E., Kaufman, D.S., and Wuest, R.A., 2007, Sediment mixing and stratigraphic disorder revealed by the age-structure of *Tellina* shells in Great Barrier Reef sediment: *Geology*, v. 35, no. 9, p. 811–814, doi: 10.1130/G23722A.1.
- Kowalewski, M., and Rimstidt, J., 2003, Average lifetime and age spectra of detrital grains: Toward a unifying theory of sedimentary particles: *Journal Of Geology*, v. 111, no. 4, p. 427–439.
- Longin, R., 1971, New method of collagen extraction for radiocarbon dating: *Nature*, v. 230, no. 5291, p. 241–242, doi:10.1038/230241a0.
- Madsen, D.B., 2000, Late Quaternary Paleoecology in the Bonneville Basin: *Utah Geological Survey Bulletin* 130.
- Miller, J.H., 2011, Ghosts of Yellowstone: Multi-Decadal Histories of Wildlife Populations Captured by Bones on a Modern Landscape: *PLoS One*, v. 6, no. 3, p. e18057, doi: 10.1371/journal.pone.0018057.g004.
- Olszewski, T.D., 2012, Remembrance of things past: modelling the relationship between species' abundances in living communities and death assemblages: *Biology letters*, v. 8, no. 1, p. 131–134, doi: 10.1098/rsbl.2011.0337.

- Terry, R.C., 2007, Inferring predator identity from skeletal damage of small-mammal prey remains: *Evol Ecol Res*, v. 9, p. 199–219.
- Terry, R.C., 2004, Owl Pellet Taphonomy: A Preliminary Study of the Post-Regurgitation Taphonomic History of Pellets in a Temperate Forest: *Palaios*, v. 19, no. 5, p. 497, doi: 10.1669/0883-1351(2004)019<0497:OPTAPS>2.0.CO;2.
- Terry, R.C., 2007, Inferring predator identity from skeletal damage of small-mammal prey remains: *Evolutionary Ecology Research*, v. 9, p. 199–219.
- Terry, R.C., 2010a, On raptors and rodents: Testing the ecological fidelity and spatiotemporal resolution of cave death assemblages: *Paleobiology*, v. 36, no. 1, p. 137–160, doi: 10.1666/0094-8373-36.1.137.
- Terry, R.C., 2010b, The dead do not lie: Using skeletal remains for rapid assessment of historical small-mammal community baselines.: *Proceedings of the Royal Society B*, v. 277, no. 1685, p. 1193–1201, doi:10.1098/rspb.2009.1984.
- Terry, R.C., Li, C.L., and Hadly, E.A., 2011, Predicting small-mammal responses to climatic warming: autecology, geographic range, and the Holocene fossil record: *Global Change Biology*, v. 17, no. 10, p. 3019–3034, doi: 10.1111/j.1365-2486.2011.02438.x.
- Tomašových, A., and Kidwell, S.M., 2011, Accounting for the effects of biological variability and temporal autocorrelation in assessing the preservation of species abundance: *Paleobiology*, v. 37, no. 2, p. 332–354, doi:10.1666/09506.1.
- Tomasovych, A., Kidwell, S.M., Foygel Barber, R., and Kaufman, D.S., 2014, Long-term accumulation of carbonate shells reflects a 100-fold drop in loss rate: *Geology*, doi: 10.1130/G35694.1.
- Western, D., and Behrensmeyer, A.K., 2009, Bone Assemblages Track Animal Community Structure over 40 Years in an African Savanna Ecosystem: *Science*, v. 324, no. 5930, p. 1061–1064, doi:10.1126/science.1171155.